11th International Workshop on Ship and Marine Hydrodynamics
Hamburg, Germany, September 22-25, 2019

Diffraction of Wavefront Around Cylinders

R.P. Li[1,*], X.B. Chen[1,2], W.Y. Duan[1]

[1]Harbin Engineering University, College of Shipbuilding Engineering
145 Nan-Tong Street, 150001 Harbin, China
[2]Bureau Veritas, Research Department
8 cours du triangle, 92937 Paris La Defense, France

[*]Corresponding author, liruipeng@hrbeu.edu.cn

ABSTRACT

The diffraction of transient waves around an infinite cylinder vertically fixed in deepwater is considered. The velocity potential and corresponding normal derivatives on the cylinder surface are expanded by the Laguerre function in vertical direction and Fourier series along the circumference. Green's Theorem is applied in the domain external to the cylinder, to obtain the so-called Dirichlet-to-Neumann (DtN) operator, which represents the relationship between series expansion coefficients related to the velocity potential and its normal derivative on the cylinder. Transient waves diffracted from any kind of incoming waves can then be obtained by applying the above DtN operator. The boundary integral equation (BIE) established in the fluid domain is a three-folds integral, two with respect to the cylinder surface and one with respect to time, and the time-domain Green function itself is a single one. In the scheme of Galerkin collocation, to obtain the DtN operator, the boundary integral equation is multiplied by a base function on both sides and integrated over the cylinder surface. A new boundary integral equation connecting the expansion coefficients related with velocity potential and normal derivative is obtained. Although all elements in the coefficients matrix are multi-folds integrals in form, they can be reduced to single ones with respect to wavenumber by using orthogonal properties of Laguerre functions and Fourier series, except for the convolution integral which can be expressed by a summation.

Unlike in classical work where steady-state plane progressive waves are involved, transient waves with wavefronts, which are generated by a wavemaker, are selected as the incoming waves in present study. Wavefront can be observed in real sea, physical wave tank and numerical simulations. A study on transient waves with wavefronts is of importance to understand better the wave diffraction by cylinders. Results from the above method are compared with those from an existing time-domain analyzing method which introduces the frequency domain solution into transient wave elevation on the free surface to express the transient diffracted waves.

1 INTRODUCTION

Reliable predictions of wave-induced motions and loads on offshore structures and ships are important to the design and operation at sea. The potential flow theory has been widely applied to solve hydrodynamic problems such as wave-current, wave-wave and wave-body interactions. Unlike volume-discretisation methods, boundary element method (BEM) is a kind of dimension-reducing strategy where unknowns are distributed on boundaries of computational domain by satisfying boundary conditions. Higher-order boundary element methods (HOBEM) are developed in [1] and it is believed to give more accurate results than the constant panel method. To improve the solution accuracy in non-smooth boundary problems, the Taylor expansion boundary element method (TEBEM) is developed in [2]. It is worth

noting that in either constant panel method or HOBEM and TEBEM, the body surface, as a part of fluid domain boundary, needs to be discretised to small panels, which makes originally continuous surface discontinuous and so does the velocity potential on the body surface. Usually, a large number of panels are needed to obtain the convergence.

Frequency domain analysis being widely used in the design stage, time domain analysis is a direct and powerful way to give detail descriptions of the real world, either in theoretical analysis or in numerical simulations. It is helpful in identifying and solving transient linear and nonlinear problems, especially for ship hydrodynamics with zero and non-zero forward speed. According to ITTC 2011 report, time domain methods are quickly replacing frequency domain methods for many practical applications, because of easy extension to nonlinear motions analysis and coupled analysis with external and internal problems. Time domain approaches [3, 4] have been developed to solve the marine hydrodynamic problems.

In the framework of BEM, Rankine panel method (RPM) and Green function method (GFM) are two mainstreams. Based on the three-dimensional time-domain RPM, some hydrodynamic codes are developed. RPM can be extended to study non-linear problems, but numerical techniques are needed to deal with the radiation condition. Free-surface Green functions, collected in [5] and applied in GFM, are fundamental solutions satisfying not only the governing equation but also free surface boundary conditions. Therefore, a source distribution is not required on the free surface in GFM. Due to the highly oscillatory property of the time-domain Green function, efforts have been made to evaluation of the free-surface Green function itself and its derivatives efficiently and accurately. Details are shown in [6] on their approximations in both time and frequency domains for both finite and infinite water depth. The representation of transient Green function by the ordinary differential equation has been found in [7]. To combine advantages of RPM and GFM, hybrid or multi-domain methods have been studied in [8–10].

Cylindrical structures are typical in the ocean engineering, such as Spar and Tension Leg Platform. Wave diffraction by a circular cylinder is therefore a fundamental and essential problem, first solved in [11] for infinite water depth and extended to finite depth in [12], and it has been widely investigated as reviewed in [13] from linear diffraction by a single cylinder to second-order diffraction by an array of cylinders. Wave diffraction by a vertical cylinder and cylinder arrays in time domain can be found in many publications, which include those by [14–16]. However, the incoming waves used in wave diffraction problem are usually in steady-state with a ramp or modulation function at the beginning stage to avoid an abrupt initial condition. To authors' knowledge, few literature discuss the wavefront giving more wave details in water waves. A study with transient incoming waves with wavefronts is important to understand better wave diffraction around cylinders and to provide benchmark results for numerical methods for structures of arbitrary geometry.

Moreover, evaluating transient wave diffraction by a cylinder is an essential block for a further application to the complete method in [10] based on domain decomposition, where a cylindrical surface is introduced at some distance from the body and concerned as a control surface in [17, 18]. The whole fluid domain is then decomposed into an interior sub-domain surrounding the body and another extending to infinity along the radial direction as the exterior one. Information between interior and exterior sub-domains will be exchanged through the DtN or inverse Neumann-to-Dirichlet (NtD) operator constructed on the analytical cylindrical control surface. RPM and GFM, which are respectively applied to interior and exterior sub-domains, are coupled to solve hydrodynamic problems in the time domain.

The layout of this paper is as follows. Section 2 summarises the Fourier-Laguerre expansion method in time domain and boundary integral equation associated with expansion coefficients is constructed in the sense of Galerkin collocation. Incoming waves with wavefronts and wave diffraction by a cylinder are also formulated. Numerical results and comparisons are shown in section 3. Finally, some concluding remarks and work ongoing are addressed in section 4.

2 BASIC FORMULATIONS

A coordinate system $Oxyz$ is introduced with the Oz axis orienting positively upwards and Oxy plane coinciding with the calm water level. The fluid is assumed inviscid, incompressible and the flow is

irrotational. The fluid velocity can be described by the gradient of a velocity potential Φ, which satisfies the Laplace equation in the fluid domain,

$$\nabla^2\Phi = 0. \tag{1}$$

We consider an infinitely deep circular cylinder with a radius c vertically fixed in deepwater with its axis coinciding with the Oz axis. The transient wave diffraction of wavefronts around the cylinder is studied in this work. We therefore introduce cylindrical coordinates (h, φ, z) with relations $(x, y) = h(\cos\varphi, \sin\varphi)$.

2.1 Incoming waves with wavefronts

Wavefronts can be observed in the generation of plane progressive waves in the physical and numerical wave tank. Different wave-maker types, like piston, swinging or flexible plate, can generate different wavefronts while the steady-state will be same as shown in [19]. In the present work, the transient incoming waves with wavefronts, studied in [20], are generated by a harmonically oscillating flexible plate locating at $x = -L$, where L is the distance between wave-maker and cylinder centre. The linear incident potential $\Phi^I(h, \varphi, z, t)$ with respect to the reference of cylinder is written as :

$$\Phi^I = \frac{Ag}{\omega}\mathrm{e}^{k_0 z}\sin(\omega t)\sin(k_0 x) + \frac{2Agk_0}{\omega\pi}\fint_0^\infty \frac{\omega \mathrm{e}^{kz}}{k^2-k_0^2}\frac{\sin(\beta t)}{\beta}\cos(kx)\,\mathrm{d}k, \tag{2a}$$

$$= \frac{2Agk_0}{\omega\pi}\int_0^\infty \frac{(\omega/\beta)\sin(\beta t)\,\mathrm{e}^{kz} - \sin(\omega t)\,\mathrm{e}^{k_0 z}}{k^2-k_0^2}\cos(kx)\mathrm{d}k, \tag{2b}$$

$$= \frac{2Agk_0}{\omega\pi}\Re\fint_0^\infty \frac{\omega \mathrm{e}^{kz}}{k^2-k_0^2}\frac{\sin(\beta t)}{\beta}\mathrm{e}^{\mathrm{i}kx}\mathrm{d}k, \tag{2c}$$

where $x = h\cos\varphi + L$, $\beta = \sqrt{gk}$ g is the gravitational acceleration, and $\Re[\cdot]$ represents to take the real part. Integral symbols $\fint$ in (2a) and $\fint\!\!\!\!\!\curvearrowright$ in (2c) stand for the Cauchy principal-value integral and the integral along a contour bypassing the pole $k = k_0$ from above, respectively. The incoming waves with amplitude A propagate in the direction of increasing x and the wave direction angle is assumed to be zero. The wave frequency ω and wavenumber k_0 are subject to the deep-water dispersion equation $\omega^2 = gk_0$. In the absence of cylinder, the non-dimensional wave elevation on the free surface can be given by the following three corresponding expressions :

$$\frac{\eta^I}{A} = \eta(x,t) = -\cos(\omega t)\sin(k_0 x) - \frac{2k_0}{\pi}\fint_0^\infty \frac{\cos(\beta t)}{k^2-k_0^2}\cos(kx)\,\mathrm{d}k, \tag{3a}$$

$$= -\frac{2k_0}{\pi}\int_0^\infty \frac{\cos(\beta t) - \cos(\omega t)}{k^2-k_0^2}\cos(kx)\mathrm{d}k. \tag{3b}$$

$$= -\frac{2k_0}{\pi}\Re\fint_0^\infty \frac{\cos(\beta t)}{k^2-k_0^2}\mathrm{e}^{\mathrm{i}kx}\mathrm{d}k. \tag{3c}$$

The contour integral (3c) is studied in [21], where the transient waves are reformulated and decomposed into the steady-state component $\eta_S(x,t)$, the initial component $\eta_T(x,t)$, the wavefront component $\eta_F(x,t)$ and the local component $\eta_L(x,t)$,

$$\eta(x,t) = \eta_S(x,t) + \eta_T(x,t) + \eta_F(x,t) + \eta_L(x,t), \tag{4}$$

where $\eta_S(x,t)$ and $\eta_T(x,t)$ exist only for $x < t/(2\omega)$. $\eta_T(x,t)$ is significant in the region near the wave-maker and at initial time. More details on characteristics of different components and behaviours of transient waves with wavefronts can be referred to [21, 22].

2.2 Establishment of BIE based on Fourier-Laguerre expansions

Applying the Green's theorem in the semi-infinite fluid domain limited by surface of the cylinder $\mathcal{C}$, the free surface $\mathcal{F}$ on the top, and a cylindrical control surface at infinity $\mathcal{S}_\infty$, we can write the velocity

potential of a flow-field point $P(x,y,z)$ as :

$$\Phi(P,t)=\int_0^t\iint_{\mathcal{C}+\mathcal{F}+\mathcal{S}_\infty}[\Phi_n(Q,\tau)G(P,t,Q,\tau)-\Phi(Q,\tau)G_n(P,t,Q,\tau)]\mathrm{d}S\mathrm{d}\tau, \tag{5}$$

where $Q(\xi,\eta,\zeta)$ represents the source point. The normal direction on all boundary surfaces is taken positively pointing into the fluid domain, and $\Phi_n=\partial\Phi/\partial n$. The Green function G defined in [5] is :

$$4\pi G(P,t,Q,\tau)=\delta(t-\tau)G^0+H(t-\tau)G^f, \tag{6}$$

representing the velocity potential at space-time (P,t) generated by the impulsive source at (Q,τ). In (6), $\delta(\cdot)$ and $H(\cdot)$ are respectively Dirac delta function and Heaviside step function; the instantaneous term G^0 and the memory term G^f are :

$$G^0=\frac{-1}{\sqrt{R^2+(z-\zeta)^2}}+\frac{1}{\sqrt{R^2+(z+\zeta)^2}}\quad\text{and}\quad G^f=-2\int_0^\infty \mathrm{e}^{k(z+\zeta)}J_0(kR)\sqrt{gk}\sin[\sqrt{gk}(t-\tau)]\mathrm{d}k, \tag{7}$$

where R is defined as $R=\sqrt{(x-\xi)^2+(y-\eta)^2}$, and $J_n(\cdot)$ denotes the mth order Bessel function of the first kind. Introducing (6) into (5), we may write :

$$4\pi\Phi(P,t)=\Phi^0(P,t)+\int_0^t\Phi^f_{\mathcal{C}}(P,t,\tau)\mathrm{d}\tau, \tag{8}$$

with the instantaneous and memory parts associated with the cylinder surface $\mathcal{C}$ being :

$$\Phi^0=\iint_{\mathcal{C}}(\Phi_nG^0-\Phi G^0_n)\mathrm{d}S\quad\text{and}\quad\Phi^f_{\mathcal{C}}=\iint_{\mathcal{C}}(\Phi_nG^f-\Phi G^f_n)\mathrm{d}S. \tag{9}$$

The integrals on $\mathcal{F}$ and $\mathcal{S}_\infty$ in the right side of (5) disappear due to the linear boundary condition on the free surface and the property of Φ at infinity. Only integrals on the cylinder surface $\mathcal{C}$ remain (9).

In traditional boundary element methods, the surface of cylinder is discretised into panels. The velocity potentials are solved on each panel due to corresponding boundary conditions. In present work, we express the velocity potential Φ and its normal derivative Φ_n analytically by some basis functions on the cylinder surface. Along the circumference, Fourier series are selected as basis function. For the present deepwater case, Laguerre polynomials are employed in the vertical direction due to their orthogonal properties in $(0,\infty)$. For the sake of simplicity, g and c have been used to define non-dimensional coordinates (h,z) by c, time t by $\sqrt{c/g}$, wavenumber k by $1/c$ and velocity potential Φ by $\sqrt{gc^3}$. On the cylinder surface $\mathcal{C}(h'=1,-\pi<\varphi'\leq\pi)$, the velocity potential Φ and corresponding normal derivative Φ_n are expanded by the Fourier-Laguerre series :

$$\Phi=\sum_{m=0}^\infty\sum_{n=-\infty}^\infty\phi_{mn}(\tau)\mathcal{L}_m(-\zeta)\mathrm{e}^{\mathrm{i}n\varphi'}\quad\text{and}\quad\Phi_n=\sum_{m=0}^\infty\sum_{n=-\infty}^\infty\psi_{mn}(\tau)\mathcal{L}_m(-\zeta)\mathrm{e}^{\mathrm{i}n\varphi'}, \tag{10}$$

in which the Laguerre function $\mathcal{L}_m(x)$ is defined by $\mathcal{L}_m(x)=\mathrm{e}^{-x/2}L_m(x)$ with $L_m(x)$ for $x\geq0$ standing for the mth order Laguerre polynomial defined in [23]. The expansion coefficients ϕ_{mn} and ψ_{mn} in (10) will be obtained from the corresponding inverse transformation and given by :

$$\{\phi_{mn}(t),\psi_{mn}(t)\}=\frac{1}{2\pi}\int_{-\infty}^0\int_{-\pi}^{\pi}\{\Phi,\Phi_n\}\,\mathcal{L}_m(-\zeta)\mathrm{e}^{-\mathrm{i}n\varphi'}\mathrm{d}\varphi'\mathrm{d}\zeta. \tag{11}$$

By substituting the Fourier-Laguerre expansions of Φ and Φ_n on the cylindrical surface $\mathcal{C}$ into Φ^0 and $\Phi^f_{\mathcal{C}}$ given in (9), a new form of the velocity potential gives :

$$\Phi(P,t)=\sum_{m=0}^\infty\sum_{n=-\infty}^\infty\psi_{mn}(t)\mathcal{G}^0_{mn}-\phi_{mn}(t)\mathcal{H}^0_{mn}+(\psi_{mn}*\mathcal{G}^f_{mn})(t)-(\phi_{mn}*\mathcal{H}^f_{mn})(t), \tag{12}$$

where notations are defined by :

$$\left\{\mathcal{G}^0_{mn}, \mathcal{H}^0_{mn}, \mathcal{G}^f_{mn}, \mathcal{H}^f_{mn}\right\} = \frac{1}{4\pi}\iint_{\mathcal{C}} \mathcal{L}_m(-\zeta)\mathrm{e}^{\mathrm{i}n\varphi'}\left\{G^0, G^0_n, G^f, G^f_n\right\}\mathrm{d}S, \tag{13}$$

and $(\psi_{mn} * \mathcal{G}^f_{mn})(t)$ means the convolution of ψ_{mn} and $\mathcal{G}^f_{mn}$, given by :

$$(\psi_{mn} * \mathcal{G}^f_{mn})(t) = \int_0^t \psi_{mn}(\tau)\mathcal{G}^f_{mn}(t-\tau)\mathrm{d}\tau, \tag{14}$$

so does the notation of $(\phi_{mn} * \mathcal{H}^f_{mn})(t)$. By constructing BIE on the cylindrical surface $\mathcal{C}$ in the sense of Galerkin collocation via multiplying a test function $\mathcal{L}_j(-z)\mathrm{e}^{-\mathrm{i}\ell\varphi}$ on both sides of (12) and then integrating over the cylinder surface, we obtain the linear system associated with the coefficients ψ_{mn} and ϕ_{mn} as follows :

$$\phi_{j\ell}(t) = \sum_{m=0}^{\infty}\sum_{n=-\infty}^{\infty} \psi_{mn}(t)\hat{\mathcal{G}}^0_{mn,j\ell} - \phi_{mn}(t)\hat{\mathcal{H}}^0_{mn,j\ell} + (\psi_{mn} * \hat{\mathcal{G}}^f_{mn,j\ell})(t) - (\phi_{mn} * \hat{\mathcal{H}}^f_{mn,j\ell})(t), \tag{15}$$

with notations defined as follows :

$$\left\{\hat{\mathcal{G}}^0_{mn,j\ell}, \hat{\mathcal{H}}^0_{mn,j\ell}, \hat{\mathcal{G}}^f_{mn,j\ell}, \hat{\mathcal{H}}^f_{mn,j\ell}\right\} = \int_{-\infty}^{0}\int_{-\pi}^{\pi}\{\mathcal{G}^0_{mn}, \mathcal{H}^0_{mn}, \mathcal{G}^f_{mn}, \mathcal{H}^f_{mn}\}\mathcal{L}_j(-z)\mathrm{e}^{-\mathrm{i}\ell\varphi}\mathrm{d}\varphi\mathrm{d}z. \tag{16}$$

Unlike the classical boundary integral equation from which the velocity potential Φ or its normal derivative Φ_n can be solved directly on each panel, a linear system established between their expansion coefficients ϕ_{mn} and ψ_{mn} in the time domain needs to be solved in present study. It can also be observed from (13) and (16) that the transient Green function is not explicitly computed but its integration on the cylindrical surface needs to be evaluated, which can be integrated analytically and further reduced to a single integral with respect to the wavenumber.

2.3 Wave diffraction

For the diffraction potential Φ^D, the boundary condition on the cylinder surface gives $\partial\Phi^D/\partial n = -\partial\Phi^I/\partial r$. The Fourier-Laguerre expansion coefficients ψ_{mn} associated with the normal derivative of diffraction potential given in (11) takes the form of :

$$\psi_{mn}(t) = \frac{1}{2\pi}\int_{-\infty}^{0}\int_{-\pi}^{\pi}\left(-\frac{\partial\Phi^I}{\partial r}\right)\mathcal{L}_m(-\zeta)\mathrm{e}^{-\mathrm{i}n\varphi'}\mathrm{d}\varphi'\mathrm{d}\zeta. \tag{17}$$

By solving the linear system (15) in the time domain, the Fourier-Laguerre expansion coefficients $\phi_{mn}(t)$ can be obtained at each time step, and the velocity potentials distributed over the surface of cylinder are also achieved by substituting ϕ_{mn} into the first equation of (10). Moreover, the whole flow field can be known by (12) derived from the Green's theorem.

Wave forces exerting on the cylinder can be generally given by :

$$\mathbf{F}^{(I,D)} = -\iint_{\mathcal{C}} p\mathbf{n}\mathrm{d}S \quad \text{with} \quad p = -\rho\frac{\partial}{\partial t}\Phi^{(I,D)}, \tag{18}$$

where $\mathbf{F}^I$ and $\mathbf{F}^D$ are called Froude-Krylov force and wave diffraction force, respectively; ρ is the fluid density and the unit normal vector on $\mathcal{C}$ is defined as before, $\mathbf{n} = \cos\varphi\mathbf{i} + \sin\varphi\mathbf{j}$. The wave diffraction force non-dimensionalised by $(\rho g A c^2)$ is :

$$\mathbf{F}^D = \mathbf{i}\frac{2\pi}{gA}\frac{\partial}{\partial t}\sum_{m=0}^{\infty}\sum_{n=-\infty}^{\infty}(-1)^m\phi_{mn}(t)\delta_{1|n|}, \tag{19}$$

from which it can be seen that only $\phi_{m(-1)}$ and ϕ_{m1} make contribution to the wave diffraction force along x axis F_x^D. For wave elevation on the free surface due to wave diffraction, the instantaneous terms $\mathcal{G}_{mn}^0$ and $\mathcal{H}_{mn}^0$ in (12) are nil when $z = 0$. Therefore,

$$\eta^D = -\frac{1}{g}\frac{\partial}{\partial t}\left[\sum_{m=0}^{\infty}\sum_{n=-\infty}^{\infty}\left[(\psi_{mn} * \mathcal{G}_{mn}^f)(t) - (\phi_{mn} * \mathcal{H}_{mn}^f)(t)\right]\right]_{z=0}. \tag{20}$$

The total wave elevation η^T can be obtained from $\eta^T = \eta^I + \eta^D$. Furthermore, the wave run-up on the cylinder is immediate when $h = 1$ in $\mathcal{G}_{mn}^f$ and $\mathcal{H}_{mn}^f$.

3 RESULTS AND DISCUSSIONS

In this section, incident waves generated by a flexible plate will be first presented, where time evolution of incoming waves with wavefronts are illustrated. Numerical results from Fourier-Laguerre expansion method mentioned in the former section and a rather different time-domain analyzing method proposed in [13] will be shown for the wave diffraction around a cylinder subjected to the above generated incoming waves. The latter method uses the frequency domain solution to express transient solutions, and we name this method ETM here. All results are obtained by using the geometric and calculation parameters: cylinder radius $c = 1$, wavenumber $k_0 = \{1.0, 3.0\}$, wave-maker location $x = -L = -4\pi$ if not specified. The time step takes $\Delta t = T/60$, where T denotes the wave period $T = 2\pi/\sqrt{gk_0}$. The maximum of terms in Fourier-Laguerre expansions are respectively 11 and 41. In the following figures with comparison, lines are obtained from ETM and square symbols are obtained from Fourier-Laguerre expansion method.

3.1 Incoming waves

The wave-maker does a harmonic motion at the equilibrium position. Figure 1a describes the waves at two fixed locations varying in time t/T. The thin and thick dot-dashed lines are obtained at $x/\lambda = -1$ and $x = 0$ with $k_0c = 1$ and $L/\lambda = 2$, respectively. λ represents the wave length $\lambda = 2\pi/k_0$. The thin solid and thick short dashed lines are time history at same location $x/\lambda = -3$ and $x = 0$ with $k_0c = 3$ and $L/\lambda = 6$, respectively. Corresponding ratios of wave length and diameter are $\lambda/(2c) = \{\pi, \pi/3\}$. Time evolution of the wave generation from initially rest to steady-state can be observed. Spatial profiles of transient waves with wavefronts are shown in Figure 1b from the same position $x = -L$. The thin and thick dot-dashed lines for $t/T = 8$ and $t/T = 16$ with $k_0c = 1$ start from $x/\lambda = -2$, while the thin solid and thick short dashed lines for $t/T = 8$ and $t/T = 16$ with $k_0c = 3$ start from $x/\lambda = -6$.

Take a further analysis of wave elevation on the free surface η^I given in (3a). According to the asymptotic analysis, when time t is sufficiently large for any fixed position, or when time t is fixed, for any position far from the wave-maker, we correspondingly have :

$$\lim_{t\to\infty}\eta(x,t) = A\sin[\omega t - k_0(x+L)], \quad \text{and} \quad \lim_{x\to\infty}\eta(x,t) = 0, \tag{21}$$

where the first equation represents steady-state plane progressive waves after some periods as shown in Figure 1a for $x = 0$ and $x = -L/2$, and the second equation approximately describes the existence of wavefronts. It can be observed that there exists a maximum of wave elevation before the waves reach steady-state.

3.2 Wave forces

When the potential Φ in (18) takes the form of Φ^I in (2a), the non-dimensional Froude-Krylov force F_x^I due to incoming waves is :

$$F_x^I = 2\pi\frac{J_1(k_0c)}{k_0c}\cos(k_0L)\cos(\omega t) - 4k_0\int_0^{\infty}\frac{J_1(kc)}{kc}\sin(kL)\frac{\cos(\beta t)}{k^2 - k_0^2}\mathrm{d}k. \tag{22}$$

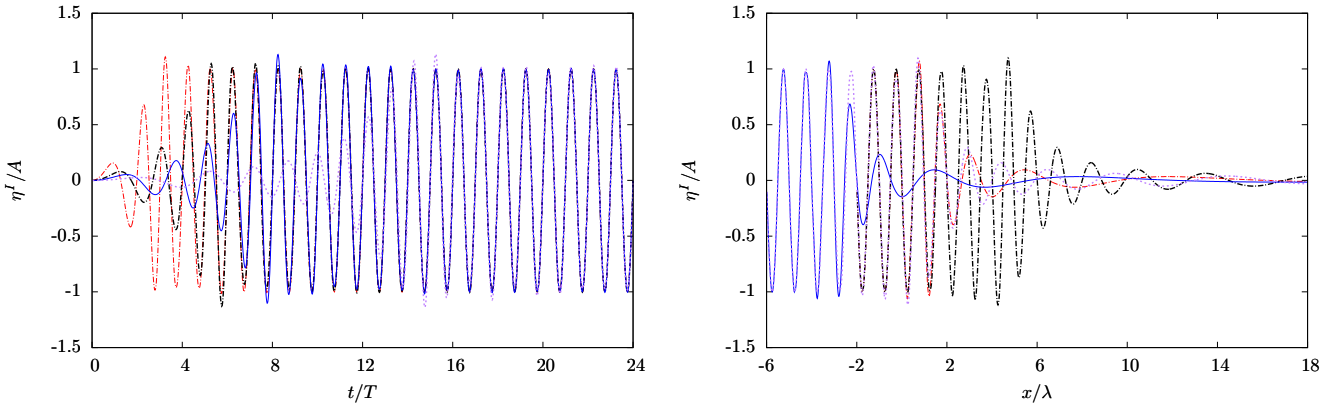

(a) (b)

Figure 1: Non-dimensional wave elevation on the free surface in the absence of cylinder, (a) varying in time t/T at two different locations and (b) varying in position x/λ at two different times. In (a), the thin and thick dot-dashed lines are for $x = -L/2$ and $x = 0$ with $k_0c = 1$, respectively. The thin solid and thick short dashed lines are for the same location with $k_0c = 3$, respectively. In (b), the thin and thick dot-dashed lines are for $t/T = 8$ and $t/T = 16$ with $k_0c = 1$. The thin solid and thick short dashed lines are for same times with $k_0c = 3$.

Adding up the above Froude-Krylov force with diffraction component defined by :

$$F_x^D = \frac{2\pi}{gA}\frac{\partial}{\partial t}\sum_{m=0}^{\infty}(-1)^m\left[\phi_{m1}(t) + \phi_{m(-1)}(t)\right], \tag{23}$$

yields the excitation force $F_x^E = F_x^I + F_x^D$, whose steady-state non-dimensional absolute value analytically known from frequency domain solutions is $|F_x^E| = 4/(k_0c)^2/|H_1^{(1)'}(k_0c)|$, where $H_n^{(1)}(kc)$ is the nth order Hankel function of the first kind, and $H_n^{(1)'}(kc)$ gives the first derivative of $H_n^{(1)}(kc)$ with respect to (kc).

Non-dimensional excitation force formulation from ETM gives :

$$F_x^E = -\frac{16}{\pi}\Re\int_0^{\infty}\frac{\omega^2\cos(\beta t) - \beta^2\cos(\omega t)}{(\beta^2-\omega^2)(\beta^2+\omega^2)}\frac{\beta e^{ikL+i\beta t'}}{(kc)^2H_1^{(1)'}(kc)}e^{-i\beta t'}d\beta, \tag{24}$$

which may be evaluated by the FFT algorithm. Wave forces exerting on the cylinder are evaluated and depicted in Figure 2a for $k_0c = 1$, $L/\lambda = 2$ and Figure 2b for $k_0c = 3$, $L/\lambda = 6$, from which it is worth noting that each wave force component varies from a non-zero value at $t = 0$. Positive initial values are due to the fact that velocity of the wave-maker is along the direction of increasing x and the pressure on cylinder beneath the free surface is not zero at the initial time $t = 0$. For further analysis on this initial value, let $t = 0$ in (22), (23) and (24). Or more explicitly, we have :

$$F_x^I\big|_{t=0} = 8\int_0^{\infty}\frac{\beta}{\beta^2+\omega^2}\frac{J_1(kc)}{kc}\sin(kL)d\beta = 4\int_0^{\infty}\frac{1}{k+k_0}\frac{J_1(kc)}{kc}\sin(kL)dk, \tag{25a}$$

and

$$F_x^E\big|_{t=0} = \frac{16}{\pi}\Re\int_0^{\infty}\frac{\beta}{\beta^2+\omega^2}\frac{e^{ikL+i\beta t'}}{(kc)^2H_1^{(1)'}(kc)}e^{-i\beta t'}d\beta = \frac{8}{\pi}\Re\int_0^{\infty}\frac{1}{k+k_0}\frac{e^{ikL}}{(kc)^2H_1^{(1)'}(kc)}dk, \tag{25b}$$

where (25b) is from ETM. The formulations illustrate relations between initial values and wavenumber k_0 and wave-maker location L. Figure 2c and Figure 2d show the initial values versus k_0c with $L = 4\pi$ and $L = 10\pi$, respectively. It can be seen that initial wave forces decrease with increasing k_0c and increasing L. Furthermore, it is worth noting that $F_x^I|_{t=0} \to \pi$ and $F_x^E|_{t=0} \to 2\pi$ with $k_0 \to 0$ in (25).

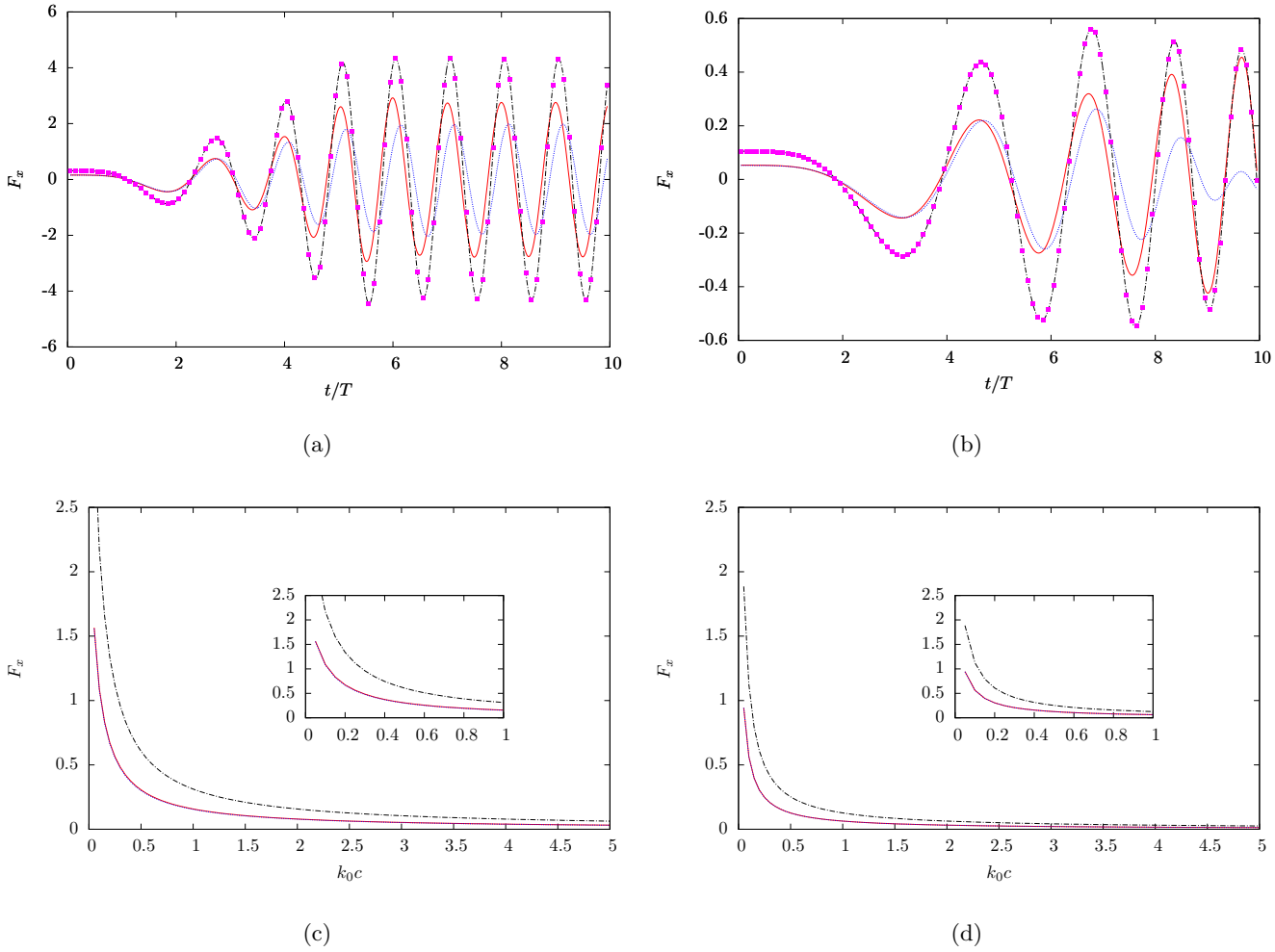

Figure 2: Non-dimensional wave forces exerting on the cylinder versus time t/T, (a) $k_0c = 1$ and $L/\lambda = 2$, (b) $k_0c = 3$ and $L/\lambda = 6$. Non-dimensional wave forces exerting on the cylinder at $t = 0$ versus k_0c, (c) wave-maker location $L = 4\pi$ and (d) $L = 10\pi$. In both (a) and (b), the square symbols representing the excitation force F_x^E, are obtained from Fourier-Laguerre expansion method. In (a-d), lines come from ETM, solid lines for the Froude-Krylov force F_x^I, dotted lines for diffraction force F_x^D and dot dashed lines for F_x^E, respectively.

3.3 Wave run-up on the cylinder

The wave run-up η_r on the cylinder due to different components are illustrated in Figure 3. The diffraction component may be obtained by :

$$\eta_r^D = -\frac{1}{g}\frac{\partial \Phi^D}{\partial t}\Big|_{z=0} = -\frac{1}{g}\frac{\partial}{\partial t}\sum_{m=0}^{\infty}\sum_{n=-\infty}^{\infty}\phi_{mn}(t)\mathrm{e}^{\mathrm{i}n\varphi}, \tag{26}$$

in which we have used $\mathcal{L}_m(0) = 1$. Non-dimensional wave elevation on the free surface from ETM gives :

$$\frac{\eta^T}{A} = \frac{4k_0}{\pi}\Re\int_0^{\infty}\frac{\cos(\omega t) - \cos(\beta t)}{(\beta^2 - \omega^2)(k + k_0)}\beta\mathrm{e}^{\mathrm{i}kL + \mathrm{i}\beta t'}\eta_f(r,\theta,k)\mathrm{e}^{-\mathrm{i}\beta t'}\mathrm{d}\beta, \tag{27}$$

where $\eta_f(\cdot)$ is defined by :

$$\eta_f(r,\theta,k) = \mathrm{e}^{\mathrm{i}kr\cos\theta} - \sum_{n=0}^{\infty}\mathrm{i}^n\epsilon_n\frac{J_n'(kc)}{H_n^{(1)'}(kc)}H_n^{(1)}(kr)\cos(n\theta), \tag{28}$$

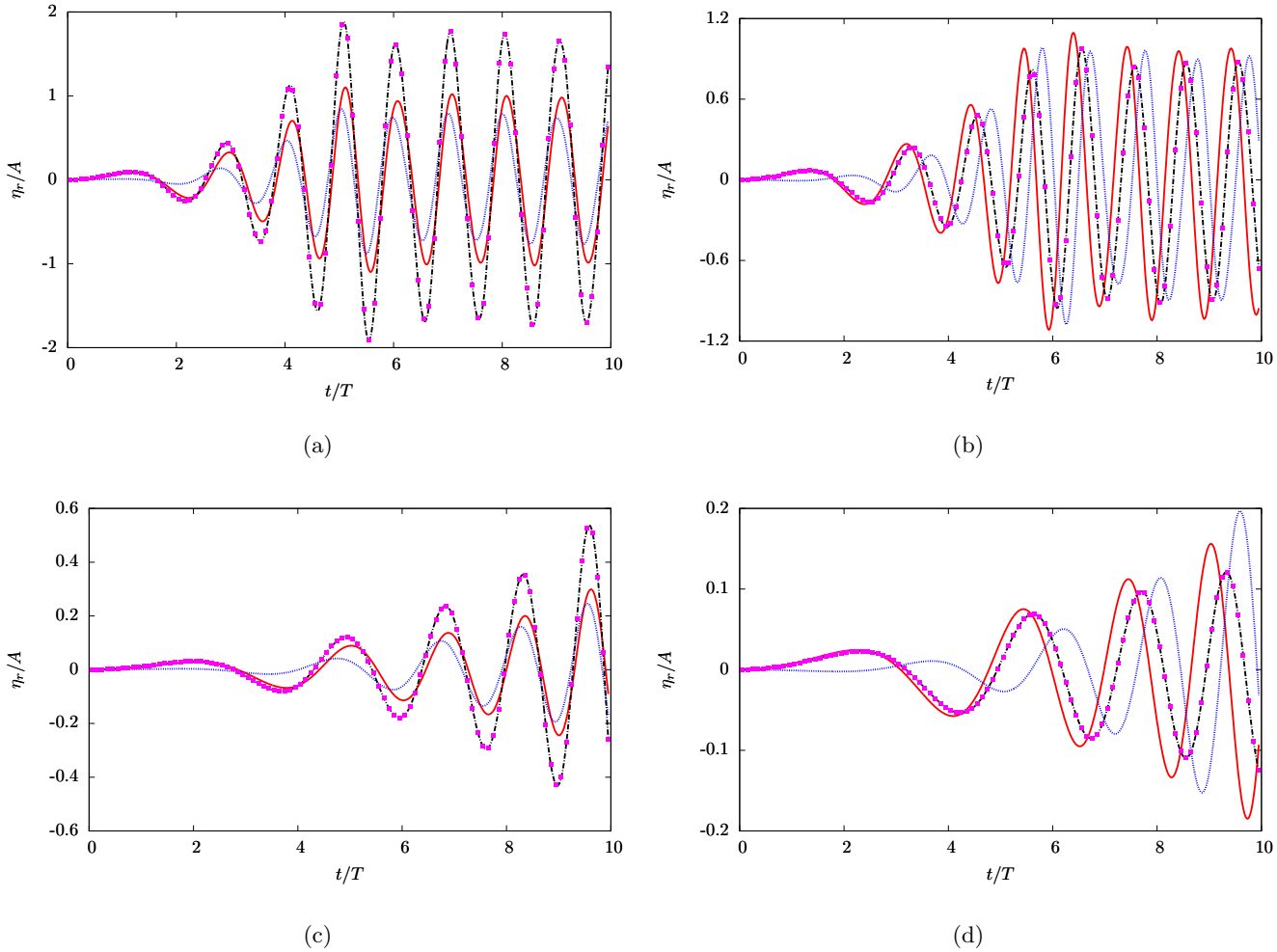

Figure 3: Wave run-up on the cylinder, non-dimensionalised by wave amplitude A, (a,b) $k_0c = 1$ and $L/\lambda = 2$, (c,d) $k_0c = 3$ and $L/\lambda = 6$, (a,c) waves at the weather side point $\varphi = \pi$ and (b,d) waves at the lee side point $\varphi = 0$. In (a-d), lines are obtained from ETM, solid lines for incoming waves, dotted lines for diffraction component and dot dashed lines for the summation of above two components. Square symbols representing total wave run-up come from Fourier-Laguerre expansion method.

with $k = \beta^2/g$, $\epsilon_0 = 1$ and $\epsilon_n = 2$ for $n \geq 1$. $J_n'(kc)$ is the first derivative of $J_n(kc)$ with respect to (kc).

Taking waves illustrated in Figure 1 as incoming waves, Figure 3a and Figure 3c show the components of a weather side point $\varphi = \pi$ on the cylinder and cases of the lee side point $\varphi = 0$ are shown in Figure 3b and Figure 3d. It can also be seen that the wave run-up on the cylinder starts from zero, which is different from wave forces. Wave run-up on the cylinder and contours of wave elevation on the free surface in vicinity of a cylinder at $t = 8T$ are depicted in Figure 4 and Figure 5, respectively. From Figure 1, it can be known that waves at $t = 8T$ with $k_0c = 3$ and $L/\lambda = 6$ have not reached to steady state. Values at the lee side point $\varphi = 0$ and the weather side point $\varphi = \pi$ are consistent with those in Figure 3. Diffraction component are illustrated in Figure 5c and total wave elevation in Figure 5d using different color scales. Curves in Figure 4 are composed by special points' values in Figure 5, which means Figure 4 has a consistency with Figure 5.

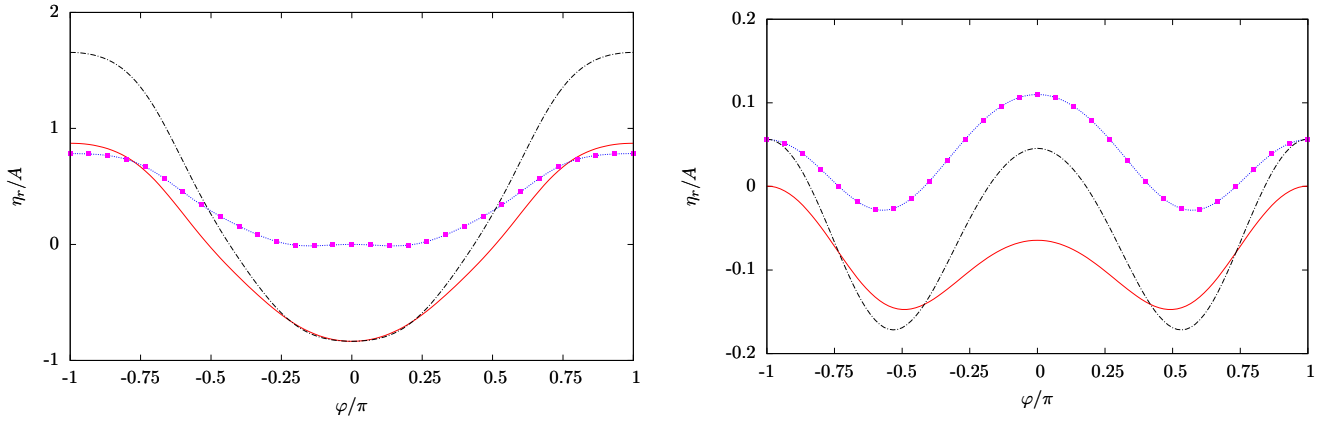

(a) (b)

Figure 4: Wave run-up on the cylinder, non-dimensionalised by wave amplitude A at $t = 8T$, (a) $k_0c = 1$, $L/\lambda = 2$ and (b) $k_0c = 3$, $L/\lambda = 6$. In both (a) and (b), the solid line is due to incoming waves. For the diffraction component, the dotted line is obtained from ETM , while the square symbols come from Fourier-Laguerre expansion method. The dot dashed line is given by the summation of incoming and diffraction components from ETM.

4 CONCLUDING REMARKS

Present study is motivated by two points. The first is to extend Fourier-Laguerre expansion method developed in [17] to the time-domain solution, which we call Fourier-Laguerre boundary element method (FLBEM). The second is to study the diffraction of wavefront by a cylinder. Unlike the traditional BEM where the cylinder surface is discretized into an ensemble of small panels cross which the unknown velocity potentials are discontinuous. As the time-domain Green function and its derivatives are highly oscillatory, a large number of panels are needed to ensure numerical convergence. The present FLBEM provides an analytical description of cylinder geometry and physical quantities by Fourier series along circumference and Laguerre functions in vertical direction, which are continuous on the body surface. Boundary integral equation associated with expansion coefficients are then established in the sense of Galerkin collocation on the cylinder surface. This FLBEM can be used in the multi-domain method proposed in [10] for wave diffraction and radiation around bodies of arbitrary geometry, to provide Dirichlet-to-Neumann operator which is the critical building block.

To verify the FLBEM in time domain, transient wave diffraction around cylinders is studied by both present FLBEM and ETM in which frequency-domain solutions are applied. In the present FLBEM, time-domain Green function is no longer explicitly evaluated. Instead, its integration involving the Fourier-Laguerre basis function on the cylinder surface is evaluated. By comparing results from these two methods, it can be concluded that the present FLBEM is valid to provide consistent results of high accuracy. Present study shows that FLBEM is able to its further application to the time-domain multi-domain method.

ACKNOWLEDGEMENTS

This work has been partially supported by the National Natural Science Foundation of China, project number 51779054.

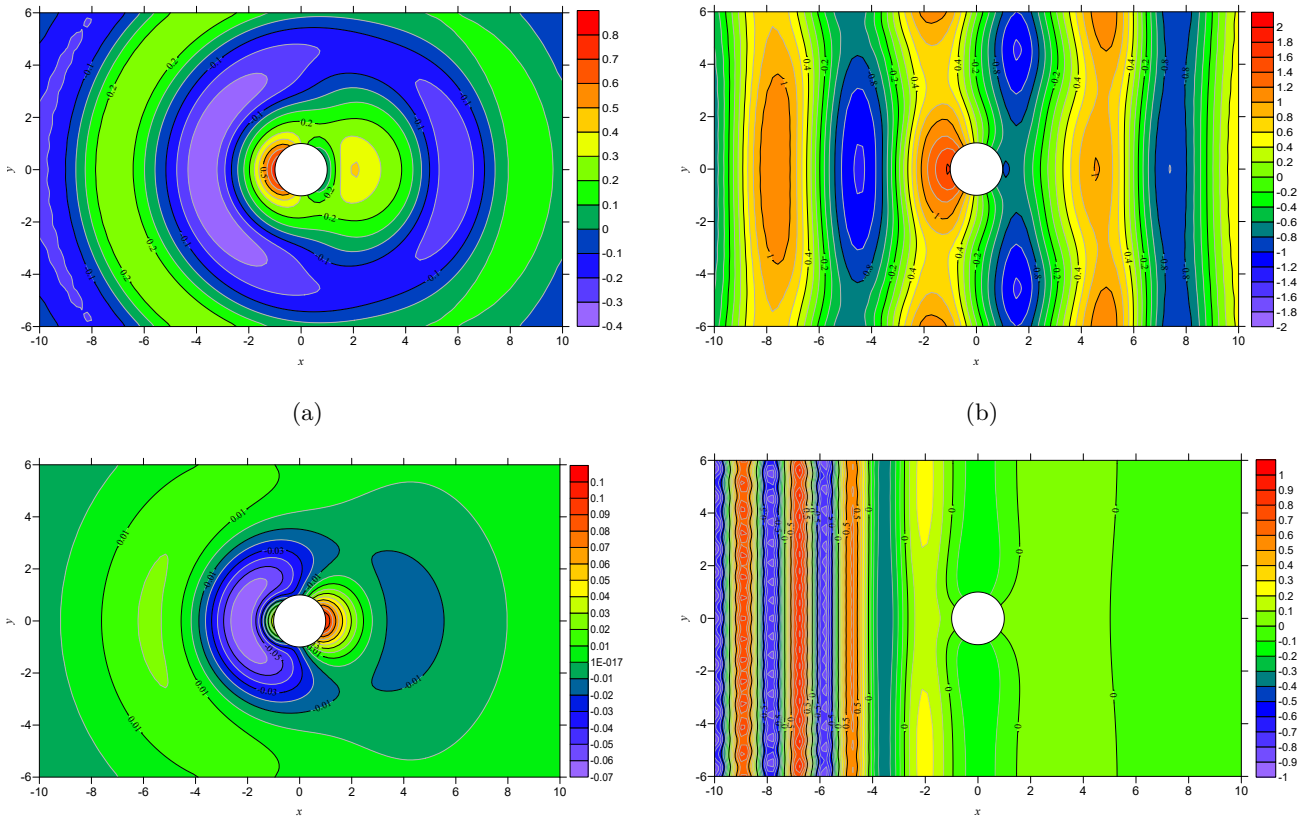

(a) (b) (c) (d)

Figure 5: Contours of wave elevation on the free surface in vicinity of a cylinder at $t = 8T$, (a,b) $k_0 c = 1$, $L/\lambda = 2$, (c,d) $k_0 c = 3$, $L/\lambda = 6$, (a,c) diffraction component and (b,d) total wave elevation.

REFERENCES

[1] B. Teng and R. Eatock Taylor. 'New higher-order boundary element methods for wave diffraction/radiation'. In: *Applied Ocean Research* 17 (1995), pp. 71–77.

[2] W. Y. Duan, J. K. Chen and B. B. Zhao. 'Second-order Taylor Expansion Boundary Element Method for the second-order wave diffraction problem'. In: *Engineering Analysis with Boundary Elements* 58 (2015), pp. 140–150.

[3] R. F. Beck and S. Liapis. 'Transient motions of floating bodies at zero forward speed'. In: *Journal of Ship Research* 31.3 (1987), pp. 164–176.

[4] D. C. Kring. 'Time domain ship motions by a three-dimensional Rankine panel method'. PhD thesis. Massachusetts Institute of Technology, 1994.

[5] J. V. Wehausen and E. V. Laitone. 'Surface waves'. In: *Hanbuch der Physik* 9 (1960).

[6] J. N. Newman. 'The approximation of free-surface Green functions'. In: *Wave Asymptotics*. Ed. by P. A. Martin and G. R. Wickham. Cambridge, UK: Cambridge Univ. Press, 1992. Chap. 4, pp. 107–135.

[7] A. H. Clément. 'An ordinary differential equation for the Green function of time-domain free-surface hydrodynamics'. In: *Journal of Engineering Mathematics* 33.2 (1998), pp. 201–217.

[8] S. K. Liu and A. D. Papanikolaou. 'Time-domain hybrid method for simulating large amplitude motions of ships advancing in waves'. In: *International Journal of Naval Architecture and Ocean Engineering* 3.1 (2011), pp. 72–79.

[9] K. Tang, R. C. Zhu, G. P. Miao and J. Fan. 'Domain Decomposition and Matching for Time-Domain Analysis of Motions of Ships Advancing in Head Sea'. In: *China Ocean Engineering* 28.4 (2014), pp. 433–444.

[10] X. B. Chen and H. Liang. 'Wavy properties and analytical modeling of free-surface flows in the development of the multi-domain method'. In: *Journal of Hydrodynamics* 28.6 (2016), pp. 971–976.

[11] T. H. Havelock. 'The pressure of water waves upon a fixed obstacle'. In: *Proceedings of the Royal Society of London A: Mathematical, Physical and Engineering Sciences* 175.963 (1940), pp. 409–421.

[12] R. C. Mac Camy and R. A. Fuchs. *Wave forces on piles: A diffraction theory*. U.S. Army Coastal Engineering Research Center (Formerly Beach Erosion Board), Technical Memorandum No. 69, 1954.

[13] R. Eatock Taylor. 'On Modelling the Diffraction of Water Waves'. In: *Ship Technology Research* 54.2 (2007), pp. 54–80.

[14] M. Isaacson and K. F. Cheung. 'Time-domain Second-order Wave Diffraction in Three Dimensions'. In: *Journal of Waterway Port Coastal and Ocean Engineering* 118.5 (1992), pp. 496–516.

[15] W. Bai and B. Teng. 'Second-Order Wave Diffraction Around 3-D Bodies by A Time-Domain Method'. In: *China Ocean Engineering* 15.1 (2001), pp. 73–84.

[16] C. Z. Wang and G. X. Wu. 'Time domain analysis of second-order wave diffraction by an array of vertical cylinders'. In: *Journal of Fluids and Structures* 23.4 (2007), pp. 605–631.

[17] H. Liang and X. B. Chen. 'A new multi-domain method based on an analytical control surface for linear and second-order mean drift wave loads on floating bodies'. In: *Journal of Computational Physics* 347 (2017), pp. 506–532.

[18] X. B. Chen, H. Liang, R. P. Li and X. Y. Feng. 'Ship seakeeping hydrodynamics by multi-domain method'. In: *Proc. 32nd Symposium on Naval Hydrodynamics, Hamburg, Germany*. 2018.

[19] S. W. Joo, W. W. Schultz and A. F. Messiter. 'An analysis of the initial-value wavemaker problem'. In: *Journal of Fluid Mechanics* 214.214 (1990), pp. 161–183.

[20] Y. S. Dai and W. Z. He. 'The Transient Solution of Plane Progressive Waves'. In: *China Ocean Engineering* 7.3 (1993), pp. 305–312.

[21] X. B. Chen and R. P. Li. 'Reformulation of wavenumber integrals describing transient waves'. In: *Journal of Engineering Mathematics* 115 (2019), pp. 121–140.

[22] X. B. Chen, B. B. Zhao and R. P. Li. 'Mysterious wavefront uncovered'. In: *Proc. 34th Intl Workshop on Water Waves and Floating Bodies, Newcastle, Australia*. 2019.

[23] M. Abramowitz and I. A. Stegun. *Handbook of Mathematical Functions: with Formulas, Graphs, and Mathematical Tables*. 55. National Bureau of Standards, 1964.